

Unconventional Berezinskii-Kosterlitz-Thouless Transition in the Multicomponent Polariton System

G. Dagvadorj,^{1,2} P. Comaron^{2,3,*} and M. H. Szymańska^{2,†}

¹*Department of Physics, University of Warwick, Coventry, CV4 7AL, United Kingdom*

²*Department of Physics and Astronomy, University College London, Gower Street, London, WC1E 6BT, United Kingdom*

³*Institute of Physics, Polish Academy of Sciences, Aleja Lotników 32/46, 02-668 Warsaw, Poland*



(Received 30 July 2022; accepted 17 February 2023; published 27 March 2023)

We study a four-component polariton system in the optical parametric oscillator regime consisting of exciton, photon, signal, and idler modes across the Berezinskii-Kosterlitz-Thouless (BKT) transition. We show that all four components share the same BKT critical point, and algebraic decay of spatial coherence with the same critical exponent. However, while the collective excitations in different components are strongly locked, both close to and far from criticality, the spontaneous creation of topological defects in the vicinity of the phase transition is found to be largely independent of the intercomponent mode locking, and instead strongly dependent on the density within a given mode. This peculiar characteristic allows us to reveal a novel state of matter, characterized by configurations of topological defects proliferating on top of a superfluid with algebraic decay of coherence, observation of which is demonstrated to be within reach of current experiments.

DOI: [10.1103/PhysRevLett.130.136001](https://doi.org/10.1103/PhysRevLett.130.136001)

The study of nonequilibrium phase transitions in driven-dissipative quantum systems became of particular interest in recent years due to the unprecedented experimental progress in realizing quantum fluids of light. In two dimensions, the onset of order is described by the celebrated Berezinskii-Kosterlitz-Thouless (BKT) mechanism [1,2], where the quasicondensate phase energy is minimized by the pairing of topological defects with opposite charge. Such a phenomenon has been investigated in a wide class of conservative systems, from ⁴He [3] to ultracold atoms [4], and in different types of confinements [5]. In the context of driven-dissipative polariton fluids [6,7], numerical studies of incoherently driven [8,9], as well as coherently driven systems in the optical parametric regime (OPO) regime [10], have predicted a nonequilibrium-type BKT phase transition, recently confirmed in an experiment [11]. Recently, the BKT physics has been theoretically investigated in lattices of nonequilibrium photon condensates [12]. Finally, the presence of further qualitative corrections to the standard BKT picture introduced by higher-order phase fluctuations treated within the Kardar-Parisi-Zhang framework [13] has been proposed [14–16].

The polariton fluids are, however, intrinsically multicomponent. They consist of excitonic, photonic and, in the case of the OPO regime, the signal, idler, and pump modes. Within the OPO picture, the polariton coherence has been previously studied theoretically [17–22] and experimentally [23,24]. At a mean-field level the sum of the signal and idler phases is locked to the spatially coherent pump phase [7]. However, by including fluctuations, such a phase

locking does not hold or is weak, especially in the vicinity of the critical point [10]. Despite that, the investigations to date were limited to the signal mode of the photonic component [10] only, while the interplay of critical features in different components is yet unrevealed. Therefore, questions regarding the multicomponent nature of the phase transition remain open: (i) How does the spatial coherence differ in the different modes, and how does this affect the BKT phase transition? (ii) How are topological defects in distinct components correlated?

In this Letter, we investigate numerically the OPO thresholds showing that the nonequilibrium BKT transition occurs simultaneously (for the same pump strength) in all four components (photonic, excitonic, signal, and idler) despite marked differences in the density of the different components. Moreover, we demonstrate that coherence is characterized by the same algebraic power-law exponent, indicating a strong phase locking between collective excitations in all modes. Interestingly, such a phase locking takes place also in the vicinity of the critical point, where strong phase fluctuations are expected to modify the mean-field picture [10]. In contrast, we discover that, unlike the collective excitations (the sound modes), the topological defects (the vortices) in different components are not strongly correlated close to the phase transition, where the density of the fluid is small, nor further from the transition for the component with the weakest density, i.e., the photonic idler mode. Remarkably, the photonic idler component is found to possess an algebraic order, characteristic of two-dimensional superfluids, in the presence of

multivortex configurations. This is possible only due to the coupling of the low-density idler mode to higher density components. To our knowledge, such a peculiar state has never been seen before. This raises questions about the importance of the interplay between sound modes and vortices in superfluid phase transitions.

System and theoretical modeling.—We use stochastic simulations based on the truncated Wigner approximation [19]. Our method considers the full two-dimensional multimode polariton field, which includes fluctuations in both density and phase, represented by complex number fields $\psi_m(\mathbf{r}, t)$, where $m = X, C$ denotes the single excitonic and photonic component, respectively, and with $\mathbf{r} = (x, y)$. The stochastic differential equations for trajectories of these fields takes the following form [7,10,19] ($\hbar = 1$):

$$id\left(\begin{array}{c} \psi_X \\ \psi_C \end{array}\right) = \left[\hat{H}_0 \left(\begin{array}{c} \psi_X \\ \psi_C \end{array}\right) + \left(\begin{array}{c} 0 \\ F \end{array}\right) \right] dt + i \left(\begin{array}{c} \sqrt{\kappa_X} dW_X \\ \sqrt{\kappa_C} dW_C \end{array} \right). \quad (1)$$

In this notation, the Hamiltonian operator

$$\hat{H}_0 = \left(\begin{array}{cc} -\frac{\nabla^2}{2m_X} + g_X |\psi_X|^2 - i\kappa_X & \Omega_R/2 \\ \Omega_R/2 & -\frac{\nabla^2}{2m_C} - i\kappa_C \end{array} \right), \quad (2)$$

is written in terms of the Rabi splitting Ω_R , the exciton-exciton interaction strength g_X , the exciton and photon mass, m_X and m_C , respectively and the damping rates κ_m . Here, we consider a homogeneous monochromatic continuous-wave pump $F(\mathbf{r}, t) = f_p \exp\{i(\mathbf{k}_p \cdot \mathbf{r} - \omega_p t)\}$ with momentum \mathbf{k}_p , strength f_p , and frequency ω_p , resonant with the bare lower-polariton dispersion, so that, as shown in Fig. 1(a), polaritons undergo parametric scattering into the signal and idler states [18] for a certain range of pump strengths f_p . dW_m are independent white complex Gaussian noise terms, with zero mean and local correlations in time and space: $\langle dW_m(\mathbf{r}, t) dW_{m'}^*(\mathbf{r}, t) \rangle = 2\delta_{m,m'} \delta_{\mathbf{r},\mathbf{r}'} dt/dV$, and $\langle dW_m(\mathbf{r}, t) dW_{m'}(\mathbf{r}, t) \rangle = 0$, where dV is the cell area of the numerical grid. The reduced Wigner density reads $|\psi_X|^2 = (|\psi_X|^2 - 1/dV)$. Physical observables can be calculated by appropriate averages over stochastic realizations.

For the numerics, we have considered specific system parameters, relevant for current experiments: $\Omega_R = 4.4$ meV, $m_C = 2.3 \times 10^{-5} m_0$, where m_0 denotes the electron mass, $\kappa_m = 0.1$ meV, and $g_X = 2 \times 10^{-3}$ meV μm^2 . We have ignored the exciton dispersion as $m_X \gg m_C$. Equations (1) are numerically implemented on a N^2 grid with $N = 256$ points and length $L = N \times a$, where $a = 0.87$ μm is the uniform grid spacing. The pump is injected at finite momentum $\mathbf{k}_p = (k_p, 0)$ in the x direction, with $k_p = 1.6$ μm^{-1} .

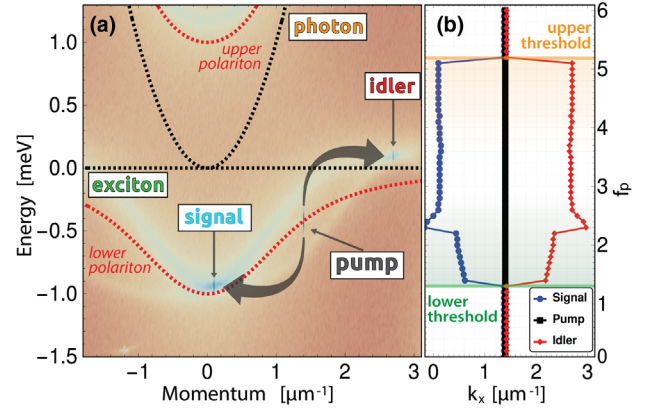


FIG. 1. Polariton OPO regime. (a) Typical spectrum of the system within the OPO window showing signal, pump, and idler modes on the lower polariton branch. (b) Signal, pump, and idler momentum k_x as a function of the pump strength f_p , exhibiting a double threshold. The ordered (disordered) phase lies in the pump range within (outside) a lower (solid green line) and an upper (solid orange line) critical point.

We evolve the stochastic equations (1) in a two-dimensional geometry with periodic boundary conditions until the steady state. While mean-field wave functions are used as initial conditions, the Wiener noise terms are adiabatically switched on along the dynamics. In driven-dissipative systems, the parameter that controls the phase transition is the pumping strength f_p , which determines the particle density. As explained in Ref. [25], once the steady state is achieved, for each m component a filtering process allows us to extract the different fields $\psi_{m,n}(\mathbf{r}, t)$, and the momenta $\mathbf{k}_{m,n}$ at which they are peaked in the momentum distribution, where $n = s, p, i$ labels the *signal*, *pump*, and *idler* mode, respectively. We ascertain that at a given pump value, the set of modes n have the same momentum structure in both components m [25]. In Fig. 1(b) we plot the behavior of the extracted momenta k_x for the photonic component, where $\mathbf{k}_{C,n} = (k_x, 0)$, as a function of the pump strength, for each mode n . Note that the OPO quasiordered phase possesses two different thresholds, easily distinguishable from Fig. 1; we extract a lower threshold (LT) at $f_p = 1.419$ and an upper threshold (UT) at $f_p = 5.149$. The ordered phase lies within the two thresholds. Further details on the filtering process, the resulting steady-state diagram, character, and identification of the critical points are reported in Ref. [25].

As discussed earlier, at the mean-field level the sum of the OPO signal and idler phases is locked to that of the external pump F . In the next sections we show how fluctuations can alter such phase locking [10], and its implications on the observation of unconventional order in a multicomponent phase transition.

Onset of multicomponent order.—We proceed by investigating the nonequilibrium phase diagram of our multicomponent system. As in previous works [8,10,26],

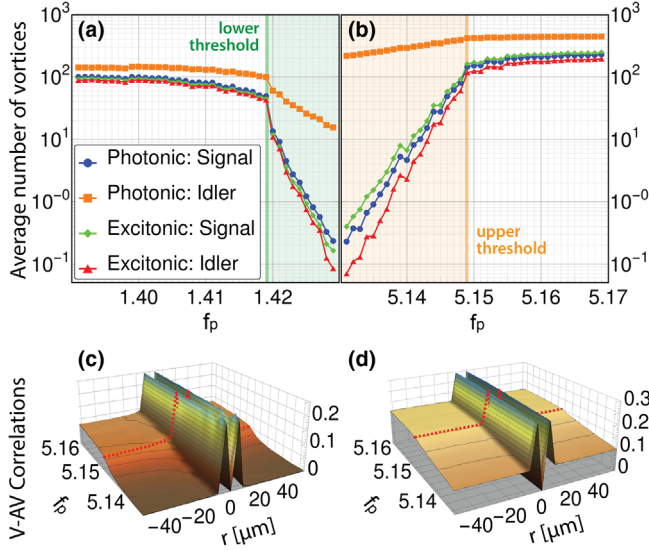


FIG. 2. Vortices near the OPO thresholds. Top: averaged number of vortices in all four components, around the (a) lower and (b) upper thresholds. The quasicondensate phase is shown as a shaded colored area. Bottom: Vortex-antivortex (V-AV) correlations at the upper threshold for the photonic component in the signal (c) and the idler (d) modes.

we calculate the average number of vortices (Fig. 2) and spatial correlation functions (Fig. 3) in the steady state close to the lower (LT) and upper (UT) phase transitions. We note that in other works, driven-dissipative phase transitions have been investigated by analyzing the excitation spectrum [22] or the fluid current-current response [27,28]. We see that, for all components, while in the disordered phases, below (above) the LT (UT), the total vortices number is large and almost constant. When the pump strength passes the critical point, the number of topological defects abruptly decrease. This is in agreement with previous results [26]: in the late dynamics, the system approaches a steady-state number of vortices, which becomes lower as one goes deeper into the ordered phase.

While we observe an abrupt change in the steady-state number of vortices at the same pump power for all components, we note that they host a different number of vortices at a given pump power—the intercomponent phase locking is not perfect in the vortex channel beyond the mean-field level. In particular, the photonic idler mode contains a number of topological defects which is, in the ordered phase, orders of magnitude larger than in the case of the other components. This can be understood by noting the difference in the particle densities [reported in Fig. 1(b) of Ref. [25]]: at small densities, characteristic of the photonic idler, critical fluctuations are relatively stronger and the creation of random vortex-antivortex pairs is more effective as compared to other higher density components. Such a behavior is in line with the observations in Refs. [8,9].

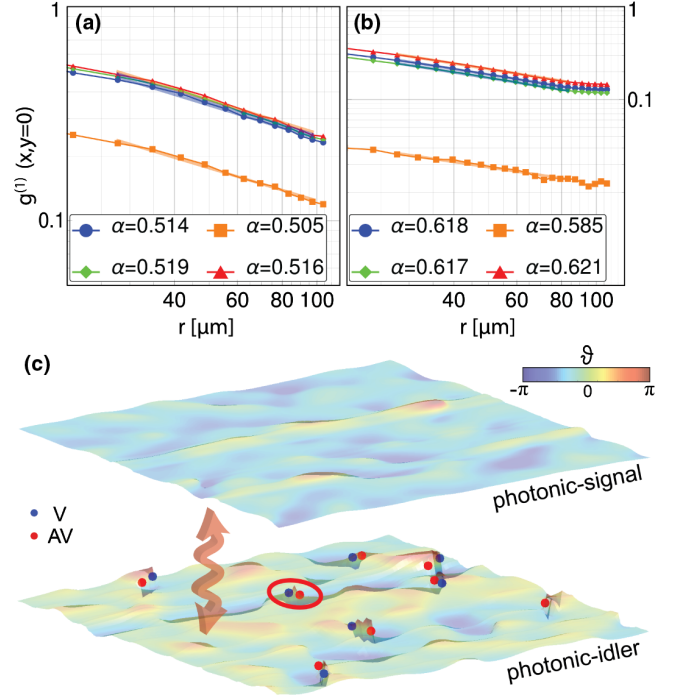


FIG. 3. Intercomponents phase locking. First order spatial correlation function along the x direction at the lower $f_{\text{th}}^{\text{low}} = 1.419$ (a) and the upper $f_{\text{th}}^{\text{up}} = 5.149$ (b) threshold. The power-law exponents α (insets) show long-range phase locking between collective modes in different components. (c) Enlarged view of the real-space phase-profiles at the lower threshold. Note, the presence (absence) of vortex configurations in the photonic idler (signal), while away from the vortices the phase still exhibits correlation between the two components.

The first order spatial correlation function in an isotropic system at a given time t , reads

$$g^{(1)}(\mathbf{r}) = \frac{\langle \psi_s^*(\mathbf{r} + \mathbf{R}) \psi_s(\mathbf{R}) \rangle_{\mathbf{R}, \mathcal{N}}}{\sqrt{\langle \psi_s^*(\mathbf{R}) \psi_s(\mathbf{R}) \rangle_{\mathbf{R}, \mathcal{N}} \langle \psi_s^*(\mathbf{r} + \mathbf{R}) \psi_s(\mathbf{r} + \mathbf{R}) \rangle_{\mathbf{R}, \mathcal{N}}}}, \quad (3)$$

where the average $\langle \dots \rangle$ is performed over the spatial position \mathbf{R} and a large number \mathcal{N} of stochastic realizations. Our numerics show that all components exhibit a phase transition from exponential to power-law decay of correlations at the same pump power, similarly to the abrupt decrease of the number of topological defects analyzed in Fig. 2. Such a transition point has been quantitatively estimated by comparing different fitting functions and choosing the best fit, as in the methods reported in Refs. [8,10]. In Fig. 3 we plot $g^{(1)}(\mathbf{r})$ (3) at the critical pump powers for the LT (a) and UT (b). Although the four modes contain very different numbers of vortices, we extract (within error bars) the same algebraic exponents, characterizing the long-range decay of $g^{(1)}(\mathbf{r})$ (3).

A detailed discussion of the difference between short- and long-range correlations is reported in Ref. [25], where we discuss how, in the photonic-idler component, coherence at small distances is destroyed by the presence of vortices but recovered at long distances by the strong intercomponent phase locking.

Motivated by the unusual observation of a high density of defects in the algebraic phase of the photonic idler, even far from the critical point, we investigate further their spatial distributions. An example of a single realization of the photonic signal and photonic idler phases is shown in Fig. 3(c). In the conventional BKT transition, away from the critical point on the quasiordered side, vortices are expected to be either fully paired or absent. On the contrary, the real space vortex configurations in the photonic idler, especially close to the upper threshold, show presence of multivortex configurations even at pump powers deep in the ordered phase (see Figs. S9-S10 and discussion in Ref. [25]). This visual observation is corroborated by the vortex-antivortex space correlations, reported in Figs. 2(c) and 2(d) and discussed in more detail in the next section.

Vortex correlations and pairing in a single component.—In order to gain a better understanding of correlations between vortices in different components, as well as the pairing of vortices and antivortices known to underly the BKT phase transition, we proceed by computing various vortex correlation functions. We define the spatial number correlators between vortex-vortex/antivortex-antivortex (hereafter denoted as V-V), and vortex-antivortex/antivortex-vortex (V-AV) as:

$$\eta_{\{V:\alpha\beta\gamma,\alpha'\beta'\gamma'\}}^{(1)}(\mathbf{r}) = \frac{\langle n_V^{\alpha\beta\gamma}(\mathbf{r}, t) n_V^{\alpha'\beta'\gamma'}(\mathbf{r} + \mathbf{R}, t) \rangle_{\mathbf{R}, \mathcal{N}}}{\sqrt{\langle N_V^{\alpha\beta\gamma} \rangle_{\mathcal{N}} \langle N_V^{\alpha'\beta'\gamma'} \rangle_{\mathcal{N}}}}, \quad (4)$$

where $n_V(\mathbf{r})$ and $\langle N_V \rangle$ are the spatial distribution and average number of vortices with components $\alpha \in \{\text{Vrx}, \text{AntV}\}$, $\beta \in \{\text{Sig}, \text{Idl}\}$ and $\gamma \in \{\text{Ph}, \text{Ex}\}$.

Let us first focus on V-AV correlations. An example is shown in panel (c) and (d) of Fig. 2, where the 3D surfaces show the correlator (4) as a function of the relative distance r as the pump power is varied across the phase transition. The threshold point is indicated as a dashed red curve on top of the 3D surface. In all cases, the correlator assumes a double peak structure with a minimum at the origin indicating V-AV attraction leading to annihilation events. In the disordered phase, characterized by a high number of free vortices, we find that V-AV correlations asymptotically approach a finite (nonzero) value as $r \rightarrow \infty$, indicating presence of vortices, whose binding nature is undetermined. In the ordered phase of the photonic signal [Fig. 2(c)], V-AV correlations plateau to a null value, indicating that on average only one tightly bound V-AV pair is left in the system. On the other hand, the ordered phase of the photonic idler [Fig. 2(d)], in agreement with

Fig. 2(a), still contains a large number of vortices as the correlator plateaus to a smaller but finite value. By visually inspecting the spatial distribution of vortices in Figs. S9-S10 of Ref. [25], we find multivortex configurations. Note, that this ensemble of vortices is mainly composed of vortex pairs; interestingly, however, we also find indication of the presence of rare free vortices. Furthermore, in Figs. S5-S6 of Ref. [25] we investigate and compare V-AV correlations in different components. We find that all components exhibit the same pairing crossover from a “randomly distributed” disordered phase to a “single-pair” ordered phase, except for the photonic idler. For pump strengths both above LT and below UT, we find a nonzero plateau indicating presence of a high number of vortices. The UT case is depicted in Fig. 2(d).

We also compute V-V correlations, which are shown and discussed in Figs. S2 and S4 of Ref. [25]. Similarly to the V-AV case, for all components other than the idler, we find a finite-valued plateau at large distances (many vortices), which crossovers to zero (single-pair) as one approaches the ordered phase. Close to the origin the autocorrelations drop to zero, indicating that vortices repel each other. Again, similarly to the V-AV, the V-V correlations also show that the photonic-idler component, even deep in the ordered phase, still shows a (lower than the one in the disordered phase, but still noticeable) finite-valued plateau.

Correlations between vortices in different components.—Considering the processes underlying the symmetry-breaking mechanism of parametric regimes—corresponding to an opposite rotation of the phases of the signal and idler components—it is expected that vortices in different modes would be “position locked” while possessing opposite circulation [19]. Vice versa, when considering vortices in the same mode (signal or idler) but different component (excitonic and photonic), the locking would take place between two vortices with same sign circulation. Following this reasoning, it is straightforward to choose the V-AV (V-V) correlations to quantify same-component (same-mode) vortex locking.

First, let us discuss the former case: signal-idler V-AV correlations are shown in Figs. 4(a) and 4(b) for the photonic and excitonic components, respectively. Here, vortex locking is easily quantified by how smooth (or peaked) the V-AV correlation profiles are across the transition: while a homogeneous profile along the r axis would indicate a similar probability of finding the V or AV partner everywhere, a peaked distribution would rather show that it is more probable to find such objects in the same position. Results shown in Figs. 4(a) and 4(b) reveal that this intermode spatial pairing mechanism takes place only for the excitonic fraction, but not for the photonic one.

A similar analysis is carried out for investigating the single-mode vortex-coupling between the excitonic and photonic components. The V-V correlator is shown in

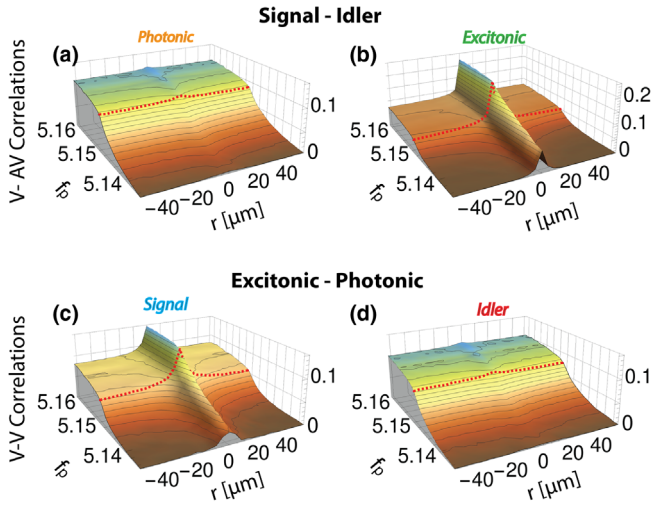


FIG. 4. Correlations between vortices in different components at the upper threshold. Top: correlation between vortices in the signal and antivortices in the idler for the photonic (a) and the excitonic (b) component. Bottom: correlation between vortices in photonic and excitonic components for signal (c) and idler (d) modes.

Fig. 4(c) for the signal and in Fig. 4(d) for the idler modes. The results reveal a strongly peaked distribution for the signal case, while the idler mode shows a smooth profile. We conclude that the spatial vortex locking between components and/or modes is always strong apart from the cases with a photonic-idler mode; this is a further confirmation of a weak vortex-locking mechanism observed for the photonic-idler component.

Vortex-antivortex correlation anisotropy.—Finally, we discuss the presence of anisotropic features in the pairing mechanism, which we observe in the vortex correlation analysis discussed above. Let us focus on the signal mode in the photonic component near the two thresholds. Figure 5 shows the V-AV correlation function in the photonic signal across the LT, along two orthogonal directions x , y . Here we see that the correlations are different along the two directions especially at short

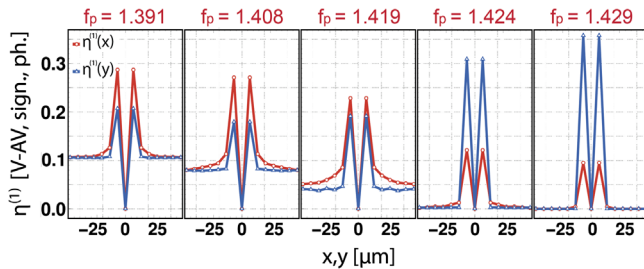


FIG. 5. Correlations between vortices and antivortices in the signal photonic component along x (red curves) and y (blue curves) directions for different pump powers across the lower threshold.

distances, pointing to anisotropic vortex antivortex interactions. At large distances, however, the correlations decay to the same offset, which is proportional to the overall vortex density. Moreover, the dominant pairing direction switches across the BKT phase transition. Near the UT, vortex correlations are instead isotropic (see Fig. S6 in Ref. [25]). To explain this behavior, we consider the possibility for the V-AV pairs to feel anisotropic forces, possibly inherited from the anisotropic pump, which is injected in the x direction. We proceed by checking the diffusion coefficients of the quantum fluid, which can be extracted by mapping the exciton-polariton model to the Kardar-Parisi-Zhang (KPZ) equation [13] for the phase. Recent works suggest that the 2D KPZ behavior could be observed in the OPO in a narrow pump-strength range in the middle of the quasiordered phase [16,29]. Note, that analytical estimates for the vortex-vortex interactions in this problem exist only for the isotropic case [30] allowing only approximate analysis. The results obtained are not conclusive (see a detailed discussion in Ref. [25]), leaving this as an exciting open question to be addressed in future works.

Conclusions.—In this Letter, we have investigated theoretically the multicomponent BKT phase transition of a two-dimensional driven-dissipative bosonic system in the OPO regime. Clear signatures of the transition from a disordered to an ordered state are inferred by computing the first order coherence, the number of vortices, and vortex correlations. We find that the critical point occurs at the same pump power with the same exponent of the algebraic decay of the first order spatial coherence function for all components. However, collective phase fluctuations (the sound modes) and the vortices are found to behave quite differently: while collective excitations are locked across all components, vortices are not perfectly spatially correlated, especially those involving the photonic idler at the upper threshold. This results in a new phase, where an algebraically ordered state exists in the presence of multivortex configurations, composed of V-AV pairs and occasionally free vortices. Such a peculiar phase is, to our knowledge, unique in the realm of condensed matter systems, and sets the basis for a novel form of superfluidity, where a low density quantum fluid is populated by topological defects, but remains in the algebraically ordered phase due to locking of the collective excitation channel to other higher density components. Our numerical findings lie in an experimentally accessible parameter window, which makes this new state experimentally verifiable. We believe our work will encourage further theoretical investigations in the direction of universal phenomena and turbulence in nonequilibrium multicomponent quantum systems.

We thank I. Carusotto, F. M. Marchetti, and A. Zamora for stimulating discussions. We thank A. Ferrier for proof-reading the manuscript. M. H. S., G. D., and P. C. gratefully

acknowledge financial support from QuantERA InterPol and EPSRC (Grants No. EP/S019669/1, No. EP/R04399X/1, and No. EP/K003623/2). P. C. acknowledges financial support from the National Science Center (Poland) Grant No. 2020/37/B/ST3/01657.

*Corresponding author.
p.comaron@ucl.ac.uk

†Corresponding author.
m.szymanska@ucl.ac.uk

- [1] V. L. Berezinskii, Zh. Eksp. Teor. Fiz. **59**, 907 (1971) [V. L. BerezinskiiSov. Phys. JETP **32**, 493 (1971)].
- [2] J. M. Kosterlitz and D. J. Thouless, J. Phys. C **6**, 1181 (1973).
- [3] D. J. Bishop and J. D. Reppy, Phys. Rev. Lett. **40**, 1727 (1978).
- [4] R. J. Fletcher, M. Robert-de-Saint-Vincent, J. Man, N. Navon, R. P. Smith, K. G. H. Viebahn, and Z. Hadzibabic, Phys. Rev. Lett. **114**, 255302 (2015).
- [5] Z. Hadzibabic, P. Krüger, M. Cheneau, B. Battelier, and J. Dalibard, Nature (London) **441**, 1118 EP (2006).
- [6] J. Kasprzak, M. Richard, S. Kundermann, A. Baas, P. Jeambrun, J. Keeling, F. Marchetti, M. Szymańska, R. Andre, J. Staehli *et al.*, Nature (London) **443**, 409 (2006).
- [7] I. Carusotto and C. Ciuti, Rev. Mod. Phys. **85**, 299 (2013).
- [8] P. Comaron, I. Carusotto, M. H. Szymańska, and N. P. Proukakis, Europhys. Lett. **133**, 17002 (2021).
- [9] Q. Mei, K. Ji, and M. Wouters, Phys. Rev. B **103**, 045302 (2021).
- [10] G. Dagvadorj, J. M. Fellows, S. Matyjaśkiewicz, F. M. Marchetti, I. Carusotto, and M. H. Szymańska, Phys. Rev. X **5**, 041028 (2015).
- [11] D. Caputo, D. Ballarini, G. Dagvadorj, C. Sánchez Muñoz, M. De Giorgi, L. Dominici, K. West, L. N. Pfeiffer, G. Gigli, F. P. Laussy, M. H. Szymańska, and D. Sanvitto, Nat. Mater. **17**, 145 EP (2017).
- [12] V. N. Gladilin and M. Wouters, Phys. Rev. A **104**, 043516.
- [13] M. Kardar, G. Parisi, and Y.-C. Zhang, Phys. Rev. Lett. **56**, 889 (1986).
- [14] E. Altman, L. M. Sieberer, L. Chen, S. Diehl, and J. Toner, Phys. Rev. X **5**, 011017 (2015).
- [15] Q. Fontaine, D. Squizzato, F. Baboux, I. Amelio, A. Lemaître, M. Morassi, I. Sagnes, L. Le Gratiet, A. Harouri, M. Wouters *et al.*, Nature (London) **608**, 687 (2022).
- [16] A. Ferrier, A. Zamora, G. Dagvadorj, and M. H. Szymańska, Phys. Rev. B **105**, 205301 (2022).
- [17] C. Ciuti, P. Schwendimann, and A. Quattropani, Phys. Rev. B **63**, 041303(R) (2001).
- [18] C. Ciuti, P. Schwendimann, and A. Quattropani, Semicond. Sci. Technol. **18**, S279 (2003).
- [19] I. Carusotto and C. Ciuti, Phys. Rev. B **72**, 125335 (2005).
- [20] M. Wouters and I. Carusotto, Phys. Rev. B **75**, 075332 (2007).
- [21] K. Dunnett and M. H. Szymańska, Phys. Rev. B **93**, 195306 (2016).
- [22] K. Dunnett, A. Ferrier, A. Zamora, G. Dagvadorj, and M. H. Szymańska, Phys. Rev. B **98**, 165307 (2018).
- [23] D. N. Krizhanovskii, D. Sanvitto, A. P. D. Love, M. S. Skolnick, D. M. Whittaker, and J. S. Roberts, Phys. Rev. Lett. **97**, 097402 (2006).
- [24] J. J. Baumberg, P. G. Savvidis, R. M. Stevenson, A. I. Tartakovskii, M. S. Skolnick, D. M. Whittaker, and J. S. Roberts, Phys. Rev. B **62**, R16247 (2000).
- [25] See Supplemental Material at <http://link.aps.org/supplemental/10.1103/PhysRevLett.130.136001> for numerical details and methods, which includes Ref. [8].
- [26] P. Comaron, G. Dagvadorj, A. Zamora, I. Carusotto, N. P. Proukakis, and M. H. Szymańska, Phys. Rev. Lett. **121**, 095302 (2018).
- [27] R. Juggins, J. Keeling, and M. Szymańska, Nat. Commun. **9**, 1 (2018).
- [28] J. Keeling, P. R. Eastham, M. H. Szymanska, and P. B. Littlewood, Phys. Rev. Lett. **93**, 226403 (2004).
- [29] A. Zamora, L. M. Sieberer, K. Dunnett, S. Diehl, and M. H. Szymańska, Phys. Rev. X **7**, 041006 (2017).
- [30] G. Wachtel, L. M. Sieberer, S. Diehl, and E. Altman, Phys. Rev. B **94**, 104520 (2016).